

# Interaction between tectonics and climate encoded in the planform geometry of stream networks on the eastern Tibetan Plateau

Minhui Li<sup>1</sup>, Hansjoerg Seybold<sup>2</sup>, Baosheng Wu<sup>3</sup>, Yi Chen<sup>4</sup>, and James W. Kirchner<sup>5</sup>

<sup>1</sup>State Key Laboratory of Hydrosience and Engineering, Department of Hydraulic Engineering, Tsinghua University

<sup>2</sup>ETH

<sup>3</sup>Tsinghua University

<sup>4</sup>State Key Laboratory of Hydrosience and Engineering, Department of Hydraulic Engineering

<sup>5</sup>ETH Zurich

December 17, 2022

## Abstract

Stream networks are highly abundant across Earth's surface, reflecting the tectonic and climatic history under which they have developed. Recent studies suggest that branching angles are strongly correlated with climatic aridity. However, the impact of tectonic forcing, especially in tectonically active regions, remains ambiguous. Here we analyze the branching angles of major stream networks on the eastern Tibetan Plateau, a region with complex tectonics, variable climate, and diverse landscapes. We find that spatial variations in tectonic uplift (as reflected in channel gradients) shape the branching geometry of stream networks on the steep eastern margin while in the flat interior of the eastern Tibetan Plateau, branching angles are mainly controlled by climatic aridity. This leads to the conclusion that, in the steep margin of the eastern Tibetan Plateau, climatic impacts on branching angles are overprinted by stronger tectonic controls.

## Hosted file

952234\_0\_art\_file\_10542243\_rmz9kt.docx available at <https://authorea.com/users/567104/articles/613609-interaction-between-tectonics-and-climate-encoded-in-the-planform-geometry-of-stream-networks-on-the-eastern-tibetan-plateau>

## Hosted file

952234\_0\_supp\_10542247\_rmz9kq.docx available at <https://authorea.com/users/567104/articles/613609-interaction-between-tectonics-and-climate-encoded-in-the-planform-geometry-of-stream-networks-on-the-eastern-tibetan-plateau>

1     **Interaction between tectonics and climate encoded in the planform**  
2     **geometry of stream networks on the eastern Tibetan Plateau**

3     Minhui Li<sup>1,2</sup>, Hansjörg Seybold<sup>2</sup>, Baosheng Wu<sup>1</sup>, Yi Chen<sup>1</sup> and James W. Kirchner<sup>2,3,4</sup>

4     <sup>1</sup> State Key Laboratory of Hydrosience and Engineering, Tsinghua University, Beijing, China

5     <sup>2</sup> Department of Environmental Systems Science, ETH Zurich, Zurich, Switzerland

6     <sup>3</sup> Swiss Federal Research Institute WSL, Birmensdorf, Switzerland

7     <sup>4</sup> Department of Earth and Planetary Science, University of California, Berkeley, CA, USA

8     Corresponding author: Baosheng Wu ([baosheng@tsinghua.edu.cn](mailto:baosheng@tsinghua.edu.cn))

9     **Key Points:**

- 10     • Branching angles of major stream networks on the eastern Tibetan Plateau  
11     vary systematically with climatic aridity and channel slopes.
- 12     • Climatic controls dominate over tectonic drivers in shaping the branching  
13     angles in the flat interior of the eastern Tibetan Plateau.
- 14     • Tectonic controls dominate over climate in shaping the branching angles in the  
15     steep margin of the eastern Tibetan Plateau.

16 **Abstract**

17 Stream networks are highly abundant across Earth’s surface, reflecting the tectonic  
18 and climatic history under which they have developed. Recent studies suggest that  
19 branching angles are strongly correlated with climatic aridity. However, the impact of  
20 tectonic forcing, especially in tectonically active regions, remains ambiguous. Here  
21 we analyze the branching angles of major stream networks on the eastern Tibetan  
22 Plateau, a region with complex tectonics, variable climate, and diverse landscapes. We  
23 find that spatial variations in tectonic uplift (as reflected in channel gradients) shape  
24 the branching geometry of stream networks on the steep eastern margin while in the  
25 flat interior of the eastern Tibetan Plateau, branching angles are mainly controlled by  
26 climatic aridity. This leads to the conclusion that, in the steep margin of the eastern  
27 Tibetan Plateau, climatic impacts on branching angles are overprinted by stronger  
28 tectonic controls.

29 **Plain Language Summary**

30 The geometry of stream networks reflects the tectonic and climatic evolution of a  
31 landscape. Prior studies show that stream branching angles tend to be wider in wetter  
32 climates. However, branching angles are also shaped by topography and thus by  
33 tectonic forcing, and the importance of climate relative to tectonics is not clear. Here  
34 we analyze branching angles of major stream networks on the eastern Tibetan Plateau,  
35 a tectonically active region where climatic aridity and channel slopes vary  
36 systematically from the relatively flat, dry interior to the steep, wet margin. The  
37 results show that stream network branching angles reflect the joint influence of  
38 tectonic forcing and climate. In the flat interior, branching angles are wider in wetter  
39 climates, consistent with previous studies in other regions. However, in the steep  
40 eastern margin, branching angles become narrower as climate becomes wetter and  
41 topographic gradients simultaneously become steeper. The shift in the relationship  
42 between angles and climatic aridity is observed in the transitional zone at intermediate  
43 topographic slopes. These results indicate that climatic controls on branching angles  
44 are gradually overwhelmed by tectonic controls as one goes from the relatively flat  
45 terrain of the interior to the steeper terrain of the tectonically active eastern margin.

46 **1. Introduction**

47 Numerous studies suggest that Earth's topography is shaped by the interplay between  
48 climate and tectonic forcing (Whittaker, 2012). River systems, for example, adjust  
49 their planform and profile geometry in response to erosion and uplift, and thus record  
50 information about a landscape's evolutionary past (Kwang et al., 2021; Perron et al.,  
51 2012; Seybold et al., 2021). Exploring the drivers that control the morphology of river  
52 systems can therefore provide insights into the processes that have shaped Earth's  
53 surface.

54 The branching angle formed by two incoming tributaries is a key morphological  
55 attribute that characterizes the planform geometry of stream networks. Thus, it may be  
56 diagnostic for the erosion processes at play and reveal how these processes vary  
57 across different tectonic and climatic zones. Recent studies have shown that mean  
58 branching angles are strongly related to climatic aridity not only across the United  
59 States (Getraer & Maloof, 2021; Seybold et al., 2017) but also globally (Seybold et al.,  
60 2018). Branching angles are typically narrower in arid regions than in humid climates,  
61 potentially indicating differences in the dominant erosion mechanisms across different  
62 climates (Seybold et al., 2017). Two distinct channel-forming processes that  
63 contribute to the headward growth of stream networks have been suggested: channel  
64 incision by surface runoff (Horton, 1945) and diffusive processes such as groundwater  
65 seepage (Dunne, 1990). Overland flow occurs when rainfall exceeds soil infiltration  
66 capacity and thus the water is routed downhill along the line of steepest descent. This  
67 phenomenon was first described by Horton (1945). Horton also observed that streams  
68 with a greater difference in slopes are more likely to branch at wider angles,  
69 consistent with steepest-descent routing of each tributary (Getraer & Maloof, 2021;  
70 Horton, 1945). Headward erosion by groundwater seepage was extensively studied by  
71 Dunne in the early 90s (Dunne, 1990). Recent theoretical studies have suggested that  
72 valley heads formed by re-emerging groundwater flow should tend to bifurcate at a  
73 characteristic angle of  $\alpha = 2\pi/5 = 72^\circ$ . This theoretical prediction is consistent with  
74 field measurements in a valley network on the Florida panhandle that is known to be  
75 formed by groundwater seepage (Devauchelle et al., 2012; Petroff et al., 2013).

76 Erosion is shaped by both climatic and tectonic forcing (Hurst et al., 2019; Whittaker,  
77 2012), and it has been widely recognized that gradients in precipitation control spatial  
78 variations in erosion rates in regions with relatively uniform tectonically-driven rock  
79 uplift rates (Ferrier et al., 2013; Henck et al., 2011; Reiners et al., 2003). In contrast,  
80 uplift and hillslope processes become major drivers of erosion rates in tectonically  
81 active margins (Harkins et al., 2007; Vance et al., 2003), potentially shaping networks'  
82 drainage patterns. Surface slope for example plays an important role in determining  
83 drainage patterns (Howard, 1967; Zernitz, 1932). Drainage patterns that occur without  
84 pronounced structural or topographic controls tend to be dendritic, with tributaries  
85 joining at wide angles (Howard, 1967). In more narrowly spaced basins, parallel  
86 drainage patterns with narrower branching angles are more common, implying that

87 regional topographic gradients influence the network's geometry (Howard, 1967;  
88 Zernitz, 1932). Jung et al. (2011) observed a transition between dendritic and parallel  
89 patterns in both natural and simulated channel networks with regional surface slopes  
90 exceeding ~3%. In arid and semi-arid regions, however, preexisting slopes seem to  
91 have no significant influence on the development of parallel or pinnate networks  
92 (Jung & Ouarda, 2017). Across the United States, Seybold et al. (2017) observed that  
93 branching angles are systematically narrower in steeper terrain, although the  
94 correlation between branching angles and channel slopes is weaker than that with  
95 aridity. However, relationships between climatic aridity, channel slopes and branching  
96 angles in tectonically active areas are less clear.

97 In order to better understand the interplay between tectonic forcing and climate in  
98 shaping a stream network's geometry, we analyze the morphology of the river systems  
99 of the eastern Tibetan Plateau. The Tibetan Plateau is a particularly interesting study  
100 area due to its strong gradients in climate and surface uplift (Clark et al., 2004). The  
101 Tibetan Plateau is located in the southwestern part of China and is often referred to as  
102 the Third Pole (Qiu, 2008). It has formed primarily due to the collision and continued  
103 convergence between the Indian and Eurasian plates (Wu, Zuza, et al., 2019) and the  
104 eastward growth of the Tibetan Plateau is thought to be driven by crustal shortening or  
105 viscous lower crustal flow (Royden et al., 2008; Tapponnier et al., 2001). The growth  
106 of the Himalayas and the Tibetan Plateau accounts for the large-scale drainage  
107 patterns of most Asian river systems (Chen et al., 2021; Clark et al., 2004; Li et al.,  
108 2022; Yang et al., 2015) which cover a wide range of different landscapes in different  
109 climatic and tectonic zones. With an average elevation of more than 4000 m above sea  
110 level, the Tibetan Plateau acts as a barrier for westerlies and monsoon circulation  
111 (Zhao et al., 2022). These topographic conditions create large climatic gradients  
112 between the plateau's arid interior and its monsoon-influenced southeast margin  
113 (Hudson & Quade, 2013). The increased precipitation, from the flat interior to the  
114 highly dissected eastern margin, is generally accompanied by steeper terrain.

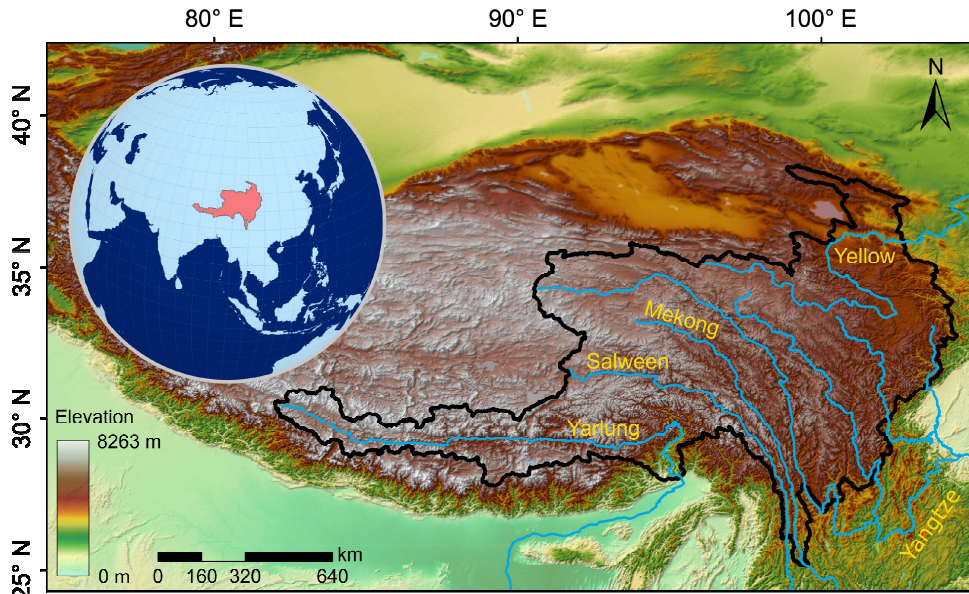
115 While the large climatic and tectonic gradients make the Tibetan Plateau a particularly  
116 interesting place for studying the influence of different controls on stream network  
117 formation, the strong coupling and feedbacks between climate and uplifted  
118 topography make it challenging to disentangle the different driving mechanisms.  
119 While our study focuses on the formation of stream network branching angles under  
120 the joint influence of climate and tectonic forcing on the eastern Tibetan Plateau, our  
121 results may also provide general clues for the development of stream networks in  
122 tectonically active regions.

## 123 **2. Data and Methods**

### 124 **2.1. Stream Networks and Branching Angles**

125 The Tibetan Plateau, known as the water tower of Asia, is the source of most of Asia's  
126 largest rivers (Immerzeel et al., 2010). Our study focuses on the river systems of the

127 eastern Tibetan Plateau, including the Yellow, Yangtze, Mekong and Salween Rivers,  
128 as well as the Yarlung (Tsangpo) River (Figure 1).



129  
130 **Figure 1.** Context map of the Tibetan Plateau showing topography and major rivers  
131 (blue lines) in our study area, the boundary of which is denoted by a solid black line.  
132 The inset shows the location of the study area on the globe.

133 The stream networks analyzed in this study have been extracted from the  
134 90-m-resolution Shuttle Radar Topography Mission Digital Elevation Model  
135 (SRTM-DEM) (<https://search.earthdata.nasa.gov/search>) using the code DEMRiver  
136 (Bai et al., 2015a; Wu, Li, et al., 2019). For the network extraction, we have set the  
137 critical source area (CSA) threshold to 40 pixels, corresponding to a drainage area of  
138 roughly 0.324 km<sup>2</sup>. Several geometric properties of stream networks such as channel  
139 slopes and Horton-Strahler (H-S) order are included in the feature calculation. In  
140 addition to the stream network, DEMRiver also provides basins and sub-basins for the  
141 different river reaches using the hierarchical pyramid method of Bai et al. (2015b)  
142 (Figure S1 in Supporting Information S1).

143 The branching angle ( $\alpha$ ) between two upstream tributaries has been calculated  
144 following the approach described by Seybold et al. (2017), which includes the  
145 following four steps. (1) We re-project the drainage networks using a conformal  
146 (angle preserving) projection. Here we use a Lambert conformal cone. (2) The  
147 projected vector segments are then converted into a series of points ordered from  
148 upstream to downstream. (3) In the next step, we fit straight lines to the two upstream  
149 tributaries using orthogonal least squares. (4) Finally, we calculate the angle between  
150 the orientation of the two regression lines.

151 In our analysis, we excluded branching angles formed by channels with negative  
152 slopes, which account for roughly 9% of the dataset and are the result of the least-cost

153 routing scheme implemented in the DEMRiver program, which allows overcoming  
154 local depressions without elevation modification. We then averaged all the branching  
155 angles within level-5 basins. Among all level-5 basins, 215 basins containing less than  
156 10 branching angles were removed from our statistics. These basins had average areas  
157 of 8 km<sup>2</sup> and mostly contained only two or three river segments. Finally, we end up  
158 with 3571 sub-basins containing a total of 789,175 branching angles. These basins  
159 have an average size of roughly ~300 km<sup>2</sup> and typically contain ~200 junctions.

## 160 **2.2. Climatic and Tectonic Metrics**

161 The Aridity Index ( $AI = P/PET$ ) is often used to describe climatic conditions because  
162 it represents the balance between precipitation ( $P$ ) and the evaporative demand of the  
163 atmosphere, as quantified by potential evaporation (PET). For our analysis of the  
164 eastern Tibetan Plateau, we calculated the mean AI value in each basin using the  
165 aridity data from the Global Aridity and PET Database (Trabucco & Zomer, 2018),  
166 which contains 30-year normals for the period 1970 to 2000 at a spatial resolution of  
167 30 arc-seconds. Note, because AI is defined as the ratio of precipitation to potential  
168 evapotranspiration, higher values of AI mean more humid conditions.

169 Tectonic forcing can create topography and maintain relief through surface uplift.  
170 Widely used topographic metrics to characterize tectonic activity are mean hillslope  
171 gradients, local relief, and in fluvial landscapes, channel steepness (Whipple, 2004).  
172 Topographic slopes have been widely used as proxies of erosional response to spatial  
173 variations in tectonic uplift rates (Kirby & Whipple, 2012; Seybold et al., 2021;  
174 Whipple, 2004). Hillslope gradients are often used to characterize surface roughness  
175 but cease to provide a proxy for erosion at high rates ( $> \sim 0.2$  mm/a) because they  
176 reach the threshold of hillslope stability (Ouimet et al., 2009). By contrast, channel  
177 slopes can be more reliable erosion proxies in rapidly eroding landscapes, because  
178 they continue to steepen with increasing erosion rates. Therefore our analysis uses  
179 mean topographic slope ( $S_t$ ) to quantify the roughness of topography and classify the  
180 eastern Tibetan Plateau into different zones, and uses channel slope ( $S_c$ ) to quantify  
181 the impact of tectonic activity on stream networks' mean branching angles.

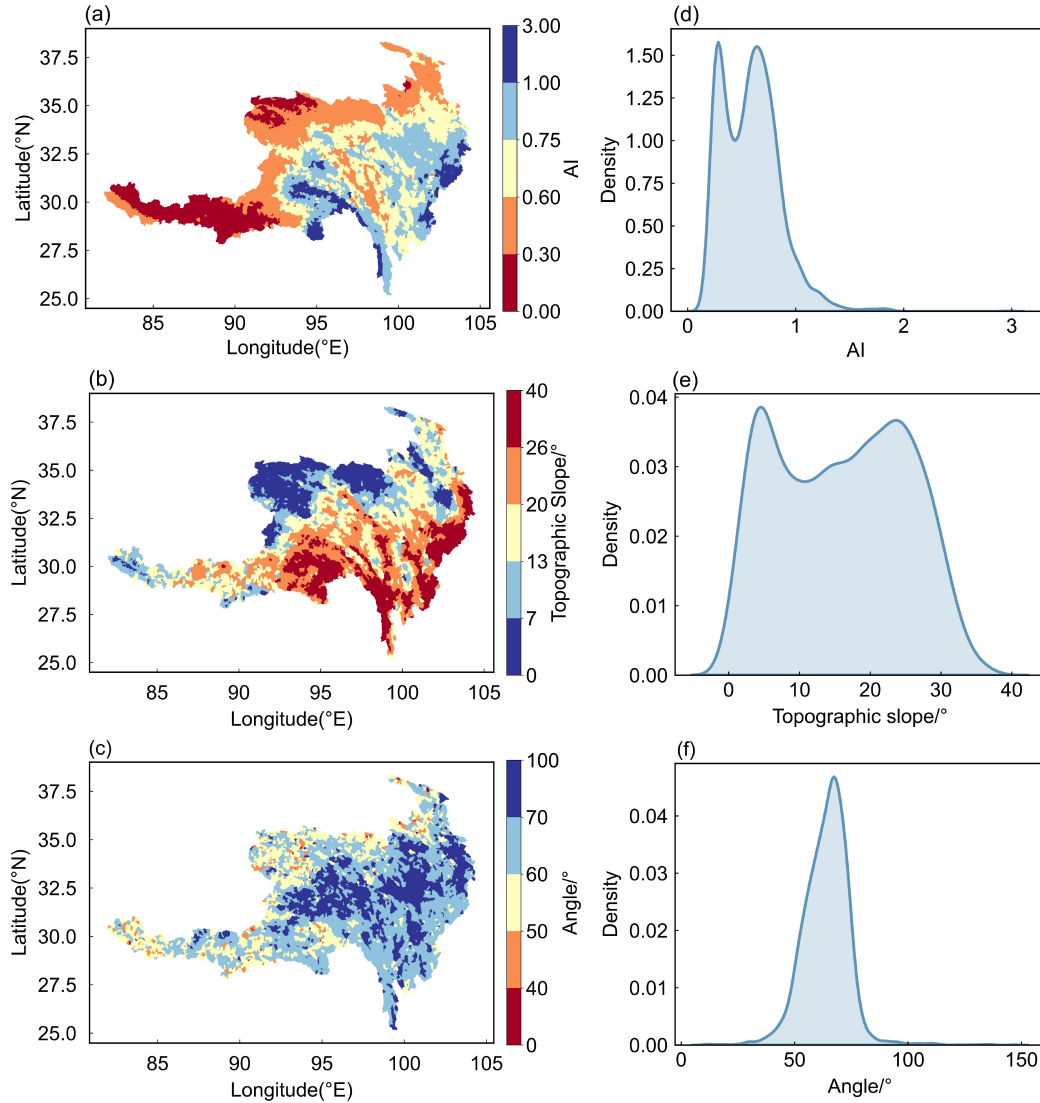
## 182 **3. Results and Discussion**

### 183 **3.1. Spatial Patterns in Branching Angles, Climate and Tectonics on the Tibetan** 184 **Plateau**

185 The spatial distributions of basin-wide averaged aridity index (AI), topographic slope  
186 ( $S_t$ ), and branching angles ( $\alpha$ ) are shown in Figure 2 (left column) together with their  
187 kernel density distributions (Figure 2, right column). Regional patterns are clearly  
188 visible, with AI values varying between 0.15 in the dry northwestern part of the  
189 eastern Tibetan Plateau and 2.96 at the most humid southeastern plateau margin  
190 (Figure 2a). Here, the deep valleys cut by the Yarlung and Salween Rivers serve as  
191 moisture paths for the South Asian Monsoon (Chen et al., 2021).

192 The deep gorges and steep rivers in the southern and eastern parts of the Tibetan  
193 Plateau reflect large gradients in exhumation rates (Wang et al., 2015; Yang et al.,  
194 2015). In the whole study area, topographic slopes and channel slopes vary widely  
195 and are highly correlated with each other (Spearman  $\rho = 0.983$ ,  $p < 0.01$ ).  
196 Topographic slopes average  $16^\circ$  and can reach up to  $37^\circ$  while channel slopes vary up  
197 to  $23^\circ$ . Except for the poorly drained low-relief areas of the Ruoergai Basin near the  
198 first bend of the Yellow River, topographic slopes tend to increase from the northwest  
199 to the southeast (Figure 2b). In the relatively low-relief interior of the Tibetan Plateau,  
200 comprising mainly the headwater areas of the Yellow, Yangtze, Mekong, and Salween  
201 Rivers, and in the Ruoergai Basin, topographic slopes are usually smaller than  $7^\circ$ .  
202 Conversely, topographic slopes increase to over  $20^\circ$  near the eastern plateau margin  
203 (Figure 2b). This high spatial variability in topographic and channel slopes also  
204 reveals the tectonic diversity of the region. On the southeastern margin of the Tibetan  
205 Plateau, Asia's big rivers have carved deep valleys into the uplifting bedrock. Deeply  
206 incised gorges and very steep rivers often coexist, which is related to zones of rapid  
207 rock uplift and incision (Hodges et al., 2001; Wang et al., 2015). In the Tsangpo Gorge,  
208 for example, the channel drops by almost  $\sim 2$  km in a stretch of less than  $\sim 50$  km  
209 (Wang et al., 2015).

210 Basin-averaged branching angles in the flat and dry interior, and in the headwaters of  
211 the Yarlung River, tend to be systematically narrower than in other regions of the  
212 study area. Additionally, the widest branching angles tend to occur in the transitional  
213 zone between the interior and the margin of the eastern Tibetan Plateau (Figure 2c).  
214 From the transitional zone towards the southeastern margin of the Tibetan Plateau,  
215 branching angles become narrower although climatic aridity AI increases. This  
216 suggests that branching angles on the eastern Tibetan Plateau may be the result of  
217 climatic signals superimposed on tectonic drivers.

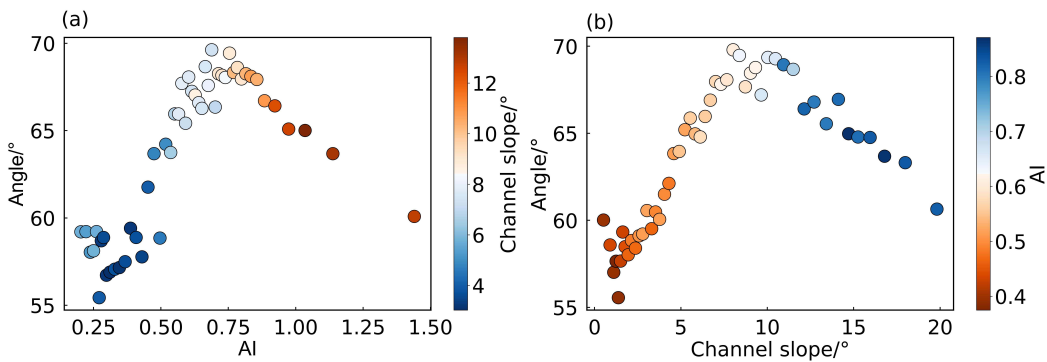


218

219 **Figure 2.** Spatial distributions of (a) basin-averaged aridity index (AI), (b)  
 220 topographic slopes ( $S_t$ ) and (c) basin-averaged branching angles ( $\alpha$ ) across our study  
 221 area. AI and  $S_t$  generally increase from northwest to southeast, reflecting more humid  
 222 climates and steeper landscapes in the southeast. Branching angles in the headwater  
 223 reaches of the major rivers are usually narrower than in the other parts. Panels (d-f)  
 224 show the corresponding kernel density distributions for AI,  $S_t$ , and  $\alpha$ .

225 To explore the interdependence of branching angles, climatic aridity (here quantified  
 226 by the aridity index AI), and tectonic forcing (here proxied by channel slope  $S_c$ ), we  
 227 first analyzed how branching angles vary with AI alone (Figure 3a). Here we averaged  
 228 the basin values into bins that each contain  $\sim 2\%$  of the data, and colored each point to  
 229 reflect the average channel slope in each bin. Average branching angles increase  
 230 systematically with increasing humidity (AI values of up to  $\approx 0.75$ ), and then start to  
 231 decrease as AI increases further. From Figure 3a we see that these humid (high-AI)

232 basins also tend to have steep channel slopes, reflecting their proximity to the steep  
 233 southeast margin of the Tibetan Plateau. A similar pattern is seen in the relationship  
 234 between branching angles and channel slopes (Figure 3b), where again each point  
 235 represents the binned mean of 2% of the data, and is colored to reflect the average AI  
 236 in each bin. In Figure 3b, mean branching angles first increase with increasing  
 237 channel slopes (as AI increases, reflecting increasing humidity), then decrease with  
 238 increasing channel slopes (as AI remains high near the southeast margin of the  
 239 Plateau). These general relations also persist after removing side-branches (Text S1  
 240 and Figure S2 in Supporting Information S1). These observations lead to the  
 241 hypothesis that strong differences in topographic uplift caused by the collision of the  
 242 Indian and Eurasian plates become a significant driver of the planform geometry of  
 243 stream networks in the wet and steep part of the eastern Tibetan Plateau.



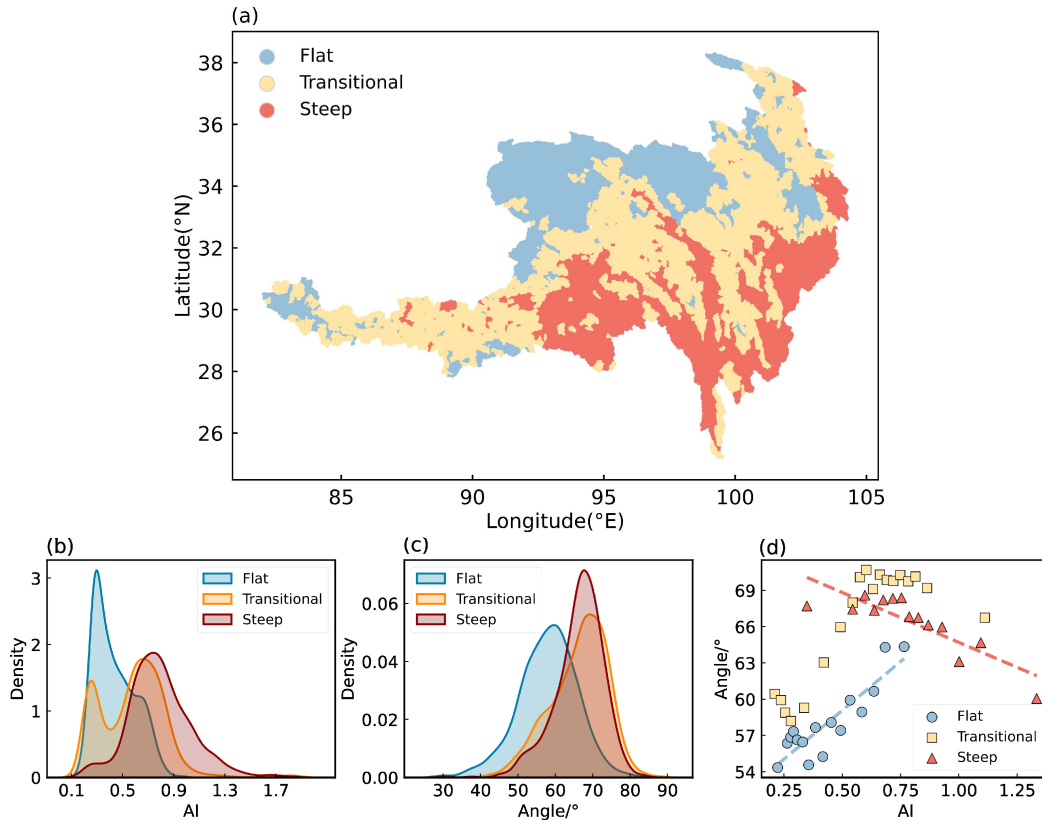
244

245 **Figure 3.** Relationships between mean branching angle and (a) aridity index AI or (b)  
 246 channel slope ( $S_c$ ). Each point contains  $\sim 2\%$  of the whole data. The color gradient in  
 247 (a) shows the variation of the average slope  $S_c$ , and in (b) it shows the variation in AI  
 248 from dry (red colors) to humid (blue colors). Branching angles increase with  
 249 increasing AI up to  $AI \approx 0.75$  and decrease as AI increases further, but points with  
 250 high AI also have high  $S_c$ . A similar pattern is found in the relationship between  
 251 branching angle and channel slopes: branching angles first increase with increasing  $S_c$   
 252 (as AI increases), and then decrease with increasing  $S_c$  (while AI remains high).

253 **3.2. Climatic and Tectonic Controls on Branching Angles in Different Slope**  
 254 **Classes**

255 To disentangle the joint influence of climate and tectonic forcing, we divide our  
 256 dataset into three zones based on topographic slope  $S_t$ . Each zone has been selected to  
 257 contain roughly the same number of basins, namely 1165 basins for  $S_t \leq 11^\circ$ , 1406  
 258 basins for  $11^\circ < S_t \leq 23^\circ$  and 1000 basins with  $S_t > 23^\circ$ . The flat catchments are  
 259 generally located in the arid (mean AI = 0.44) interior of the eastern Tibetan Plateau,  
 260 while the steep catchments are found along the humid (mean AI = 0.79) plateau  
 261 margins, and the transitional catchments have intermediate climate (mean AI = 0.58)  
 262 and are typically found between the flat and steep zones (Figure 4a). The kernel  
 263 density distributions of AI and branching angles in the three different zones are shown

264 in Figures 4b and 4c respectively. Branching angles systematically increase with AI  
 265 (Spearman  $\rho = 0.31$  and  $0.48$  respectively,  $p < 0.001$ , Figure 4d) in the flat and  
 266 transitional catchments. By contrast, the steep catchments exhibit a systematic  
 267 decrease of  $\alpha$  with AI (Spearman  $\rho = -0.24$ ,  $p < 0.001$ ) and a strong negative  
 268 correlation between  $\alpha$  and channel gradient (Spearman  $\rho = -0.48$ ,  $p < 0.001$ , Table S1  
 269 in Supporting Information S1). These results suggest that the channel slope effect on  
 270 branching angles overprints climatic controls in the steep and tectonically active  
 271 terrain of the eastern Tibetan Plateau.



272

273 **Figure 4.** (a) Spatial distributions of three topographic slope classes: flat (blue),  
 274 transitional (yellow) and steep (red). The classification roughly follows a trend from  
 275 northwest to southeast. (b and c) Kernel density estimate plots of aridity index AI and  
 276 branching angle  $\alpha$ . (d) Relationships between the basin-averaged  $\alpha$  and AI in the three  
 277 different topographic slope classes. In the flat catchments, found primarily in the  
 278 interior of the Tibetan Plateau,  $\alpha$  systematically increases with AI, while the steep  
 279 catchments, found primarily along the southeast margin of the Plateau, show a  
 280 systematic decrease of  $\alpha$  with AI.

281 The relationship between AI, channel slopes ( $S_c$ ) and branching angles ( $\alpha$ ) can also be  
 282 quantified by a multiple regression model,

283 
$$\alpha = \beta_0 + \beta_1 AI + \beta_2 S_c + \beta_3 (AI \cdot S_c) \quad (1)$$

284 where the branching angle  $\alpha$  is approximated as a linear function of AI,  $S_c$ , and their  
 285 interaction (denoted by  $AI \cdot S_c$ ), with  $\beta_i$  indicating the regression coefficients. We used  
 286 z-scores of each variable in Equation (1) and applied this model to the whole study  
 287 area, and also separately to the flat, transitional, and steep catchments.

288 Across the dataset as a whole, we find that AI and channel slopes are strongly  
 289 interdependent (Spearman  $\rho = 0.527$ ,  $p < 0.001$ ), and thus their interaction term has a  
 290 strong effect on the overall relationship between branching angles and climatic (AI)  
 291 and tectonic ( $S_c$ ) influences. Across our whole study area, AI and channel slope  
 292 account for roughly 30% of the observed variance in basin-averaged branching angles  
 293 (Table 1). While AI and channel slopes are positively correlated with branching angles,  
 294 the regression coefficient of their interaction term is strongly negative, and this  
 295 negative effect may reverse the apparent correlation that one sees when branching  
 296 angles are plotted as functions of AI or channel slope alone. AI has the strongest  
 297 control on basin-averaged branching angles ( $\beta = 0.79$ ,  $p < 0.001$ ) in the flat  
 298 catchments but does not significantly influence branching angles in the steep  
 299 catchments ( $\beta = -0.07$ ,  $p > 0.1$ ). Conversely, in the steep catchments, channel slope is  
 300 the dominant factor ( $\beta = -0.43$ ,  $p < 0.001$ ) in controlling the networks' branching  
 301 angles and thus overprints the positive relationship between branching angles and AI.  
 302 The interaction term between AI and channel slopes is insignificant in both the flat  
 303 and steep topography classes (Table 1), with  $p > 0.1$ . These results indicate that the  
 304 interaction effect of AI and channel slopes is weaker (and thus the effects of AI and  
 305 channel slopes are more clearly expressed) when flat and steep catchments are  
 306 considered separately.

307 **Table 1.** Multiple regression parameters for the whole Eastern Tibetan Plateau dataset  
 308 (ETP) and different topographic slope classes. Regression parameters with  $p < 0.001$   
 309 are shown in italics.

	ETP	Flat	Transitional	Steep
AI	<i>0.37</i>	<i>0.79</i>	<i>0.42</i>	-0.07
$S_c$	<i>0.24</i>	-0.19	<i>0.25</i>	<i>-0.43</i>
$AI \cdot S_c$	<i>-0.46</i>	0.27	<i>-0.51</i>	-0.10
R-squared	0.304	0.117	0.256	0.253

#### 310 **4. Conclusions**

311 In this study, we evaluated the relative dominance of climatic aridity and channel  
 312 slope in shaping the branching angles of stream networks on the eastern Tibetan  
 313 Plateau. Our analysis shows that spatial patterns in average branching angles reflect  
 314 spatial gradients in climatic aridity and channel slope. On the eastern Tibetan Plateau,

315 the correlation between branching angles and climatic aridity reverses between the  
316 relatively flat interior and the steep eastern margin. In the flat interior, branching  
317 angles primarily reflect variations in climatic aridity, consistent with prior studies.  
318 Going from the flat interior to the steep margin, tectonic forcing becomes increasingly  
319 important as a control on branching angle variability, leading to an inverse correlation  
320 between branching angles and climatic aridity. These findings demonstrate the joint  
321 influence of tectonic forcing and climate in shaping river network morphology.

### 322 **Acknowledgments**

323 This study was partly supported by the National Natural Science Foundation of China  
324 (No. 51639005). Minhui Li acknowledges support from the Chinese Scholarship  
325 Council.

### 326 **Data Availability Statement**

327 The dataset used to produce our results is accessible in Data at  
328 [https://figshare.com/articles/dataset/Branching\\_angles\\_on\\_ETP\\_csv/21728126](https://figshare.com/articles/dataset/Branching_angles_on_ETP_csv/21728126).

### 329 **References**

- 330 Bai, R., Li, T. J., Huang, Y. F., Li, J. Y., & Wang, G. Q. (2015a). An efficient and  
331 comprehensive method for drainage network extraction from DEM with billions of  
332 pixels using a size-balanced binary search tree, *Geomorphology*, 238, 56-67.
- 333 Bai, R., Li, T. J., Huang, Y. F., Li, J. Y., Wang, G. Q., & Yin, D. Q. (2015b). A  
334 hierarchical pyramid method for managing large-scale high-resolution drainage  
335 networks extracted from DEM, *Computers & Geosciences*, 85, 234-247.
- 336 Chen, Y., Wu, B., Xiong, Z., Zan, J., Zhang, B., Zhang, R., et al. (2021). Evolution of  
337 eastern Tibetan river systems is driven by the indentation of India, *Communications*  
338 *Earth & Environment*, 2(1), 1-7.
- 339 Clark, M. K., Schoenbohm, L. M., Royden, L. H., Whipple, K. X., Burchfiel, B. C.,  
340 Zhang, X., et al. (2004). Surface uplift, tectonics, and erosion of eastern Tibet from  
341 large-scale drainage patterns, *Tectonics*, 23(1).
- 342 Devauchelle, O., Petroff, A. P., Seybold, H. F., & Rothman, D. H. (2012).  
343 Ramification of stream networks, *Proceedings of the National Academy of Sciences*  
344 *of the United States of America*, 109(51), 20832-20836.
- 345 Dunne, T. (1990). Hydrology, mechanics, and geomorphic implications of erosion by  
346 subsurface flow, *Groundwater geomorphology: The role of subsurface water in*  
347 *earth-surface processes and landforms*, 252, 1-28.
- 348 Ferrier, K. L., Huppert, K. L., & Perron, J. T. (2013). Climatic control of bedrock  
349 river incision, *Nature*, 496(7444), 206-+.
- 350 Getraer, A., & Maloof, A. C. (2021). Climate-Driven Variability in Runoff Erosion  
351 Encoded in Stream Network Geometry, *Geophysical Research Letters*, 48(3).

- 352 Harkins, N., Kirby, E., Heimsath, A., Robinson, R., & Reiser, U. (2007). Transient  
353 fluvial incision in the headwaters of the Yellow River, northeastern Tibet, China,  
354 *Journal of Geophysical Research-Earth Surface*, 112(F3).
- 355 Henck, A. C., Huntington, K. W., Stone, J. O., Montgomery, D. R., & Hallet, B.  
356 (2011). Spatial controls on erosion in the Three Rivers Region, southeastern Tibet  
357 and southwestern China, *Earth and Planetary Science Letters*, 303(1-2), 71-83.
- 358 Hodges, K. V., Hurtado, J. M., & Whipple, K. X. (2001). Southward extrusion of  
359 Tibetan crust and its effect on Himalayan tectonics, *Tectonics*, 20(6), 799-809.
- 360 Horton, R. E. (1945). Erosional Development of Streams and Their Drainage Basins -  
361 Hydrophysical Approach to Quantitative Morphology, *Geological Society of  
362 America Bulletin*, 56(3), 275-370.
- 363 Howard, A. D. (1967). Drainage analysis in geologic interpretation: a summation,  
364 *Aapg Bulletin*, 51(11), 2246-2259.
- 365 Hudson, A. M., & Quade, J. (2013). Long-term east-west asymmetry in monsoon  
366 rainfall on the Tibetan Plateau, *Geology*, 41(3), 351-354.
- 367 Hurst, M. D., Grieve, S. W. D., Clubb, F. J., & Mudd, S. M. (2019). Detection of  
368 channel-hillslope coupling along a tectonic gradient, *Earth and Planetary Science  
369 Letters*, 522, 30-39.
- 370 Immerzeel, W. W., van Beek, L. P. H., & Bierkens, M. F. P. (2010). Climate Change  
371 Will Affect the Asian Water Towers, *Science*, 328(5984), 1382-1385. doi:  
372 10.1126/science.1183188.
- 373 Jung, K., & Ouarda, T. B. M. J. (2017). Classification of drainage network types in  
374 the arid and semi-arid regions of Arizona and California, *Journal of Arid  
375 Environments*, 144, 60-73.
- 376 Jung, K. C., Niemann, J. D., & Huang, X. J. (2011). Under what conditions do parallel  
377 river networks occur? *Geomorphology*, 132(3-4), 260-271.
- 378 Kirby, E., & Whipple, K. X. (2012). Expression of active tectonics in erosional  
379 landscapes, *Journal of Structural Geology*, 44, 54-75. doi:  
380 10.1016/j.jsg.2012.07.009.
- 381 Kwang, J. S., Langston, A. L., & Parker, G. (2021). The role of lateral erosion in the  
382 evolution of nondendritic drainage networks to dendricity and the persistence of  
383 dynamic networks, *Proceedings of the National Academy of Sciences of the United  
384 States of America*, 118(16).
- 385 Li, M. H., Wu, B. S., Chen, Y., & Li, D. (2022). Quantification of river network types  
386 based on hierarchical structures, *Catena*, 211.
- 387 Ouimet, W. B., Whipple, K. X., & Granger, D. E. (2009). Beyond threshold hillslopes:  
388 Channel adjustment to base-level fall in tectonically active mountain ranges,  
389 *Geology*, 37(7), 579-582. doi: 10.1130/g30013a.1.

- 390 Perron, J. T., Richardson, P. W., Ferrier, K. L., & Lapotre, M. (2012). The root of  
391 branching river networks, *Nature*, 492(7427), 100-+.
- 392 Petroff, A. P., Devauchelle, O., Seybold, H., & Rothman, D. H. (2013). Bifurcation  
393 dynamics of natural drainage networks, *Philosophical Transactions of the Royal  
394 Society a-Mathematical Physical and Engineering Sciences*, 371(2004).
- 395 Qiu, J. (2008). China: The third pole, *Nature*, 454(7203), 393-396. doi:  
396 10.1038/454393a.
- 397 Reiners, P. W., Ehlers, T. A., Mitchell, S. G., & Montgomery, D. R. (2003). Coupled  
398 spatial variations in precipitation and long-term erosion rates across the Washington  
399 Cascades, *Nature*, 426(6967), 645-647.
- 400 Royden, L. H., Burchfiel, B. C., & van der Hilst, R. D. (2008). The geological  
401 evolution of the Tibetan plateau, *Science*, 321(5892), 1054-1058. doi:  
402 10.1126/science.1155371.
- 403 Seybold, H., Rothman, D. H., & Kirchner, J. W. (2017). Climate's watermark in the  
404 geometry of stream networks, *Geophysical Research Letters*, 44(5), 2272-2280.
- 405 Seybold, H., Berghuijs, W. R., Prancevic, J. P., & Kirchner, J. W. (2021). Global  
406 dominance of tectonics over climate in shaping river longitudinal profiles, *Nature  
407 Geoscience*, 14(7), 503-+.
- 408 Seybold, H. J., Kite, E., & Kirchner, J. W. (2018). Branching geometry of valley  
409 networks on Mars and Earth and its implications for early Martian climate, *Science  
410 Advances*, 4(6).
- 411 Tapponnier, P., Xu, Z. Q., Roger, F., Meyer, B., Arnaud, N., Wittlinger, G., & Yang, J.  
412 S. (2001). Geology - Oblique stepwise rise and growth of the Tibet plateau, *Science*,  
413 294(5547), 1671-1677.
- 414 Trabucco, A., & Zomer, R. J. (2018). Global aridity index and potential  
415 evapotranspiration (ET0) climate database v2, *CGIAR Consort Spat Inf*, 10, m9.
- 416 Vance, D., Bickle, M., Ivy-Ochs, S., & Kubik, P. W. (2003). Erosion and exhumation  
417 in the Himalaya from cosmogenic isotope inventories of river sediments, *Earth and  
418 Planetary Science Letters*, 206(3-4), 273-288.
- 419 Wang, P., Scherler, D., Liu-Zeng J., Mey, J., Avouac, J. P., Zhang, Y. D., & Shi, D. G.  
420 (2014). Tectonic control of Yarlung Tsangpo Gorge revealed by a buried canyon in  
421 Southern Tibet, *Science*, 346(6212), 978-981.
- 422 Whipple, K. X. (2004). Bedrock rivers and the geomorphology of active orogens,  
423 *Annual Review of Earth and Planetary Sciences*, 32, 151-185. doi:  
424 10.1146/annurev.earth.32.101802.120356.
- 425 Whittaker, A. C. (2012). How do landscapes record tectonics and climate?  
426 *Lithosphere*, 4(2), 160-164.

- 427 Wu, C., Zuza, A. V., Zhou, Z. G., Yin, A., McRivette, M. W., Chen, X. H., et al.  
428 (2019). Mesozoic-Cenozoic evolution of the Eastern Kunlun Range, central Tibet,  
429 and implications for basin evolution during the Indo-Asian collision, *Lithosphere*,  
430 *11*(4), 524-550.
- 431 Wu, T., Li, J. Y., Li, T. J., Sivakumar, B., Zhang, G., & Wang, G. Q. (2019).  
432 High-efficient extraction of drainage networks from digital elevation models  
433 constrained by enhanced flow enforcement from known river maps,  
434 *Geomorphology*, *340*, 184-201.
- 435 Yang, R., Willett, S. D., & Goren, L. (2015). In situ low-relief landscape formation as  
436 a result of river network disruption, *Nature*, *520*(7548), 526-+.
- 437 Zernitz, E. R. (1932). Drainage patterns and their significance, *Journal of Geology*,  
438 *40*(6), 498-521.
- 439 Zhao, R., Fu, P., Zhou, Y., Xiao, X. M., Grebby, S., Zhang, G. Q., et al. (2022).  
440 Annual 30-m big Lake Maps of the Tibetan Plateau in 1991-2018, *Scientific Data*,  
441 *9*(1).